Supplemental Digital Content 1

Effects of Tidal Recruitment and Functional Variables on Regional Inflammation

A number of mechanical and physiologic factors besides tidal lung strain may influence the local lung inflammatory response to mechanical ventilation, and may therefore act as potential confounders in studying the inflammatory effects of regional tidal strain. For example, cyclic intra-tidal recruitment of alveoli and/or airways can trigger inflammation in airspaces (1). Additionally, average lung inflation level and hyperinflation may influence the development of inflammation through mechanical effects (2), perfusion distribution may affect both trafficking of neutrophils (3) and local exposure to LPS and circulating inflammatory mediators (4), and atelectasis can locally amplify mechanical forces (5), potentially contributing to inflammation in poorly-aerated lung regions (6). In addition, intra-regional heterogeneity of strain has been increasingly emphasized as a potential contributor to development of injury (7-9). Therefore, we estimated the degree to which each of these factors was present in the studied regions, in order to evaluate their associations with regional inflammation.

Estimation of Regional Tidal Recruitment and Functional Variables

In each of six regions-of-interest (ROIs) in all animals (delineated as described in the main text, see Figure 1A), the following variables were quantified:

1. *Fractional Tidal Recruitment (F_{TR}) of Low Aeration Compartments* – these variables were estimated using respiratory-gated images of fractional gas content at end-expiration (F_{EE}) and end-inspiration (F_{EI}). Recruitment of distinct aeration compartments was defined as the change between end-expiration and end-inspiration

of the regional fraction of lung within those compartments. We defined three aeration compartments, corresponding to non-aerated and poorly-aerated tissue defined with CT density measurements (10). Non-aerated tissue was defined as being composed of voxels with $F_{GAS}<0.1$, and poorly-aerated tissue was subdivided into two compartments consisting of $0.1<F_{GAS}<0.3$ and $0.3<F_{GAS}<0.5$. In each ROI, the fraction of voxels within each of those compartments was computed both at end-expiration and end-inspiration. The fractional tidal recruitment of each compartment was then defined as the decrease in the fraction of voxels in each compartment occurring during inspiration.

2. *Regional Perfusion per Unit Tissue ($\dot{Q}_{TIS}$)* – the regional fraction of total perfusion was estimated from ^{13}NN infusion scans as the ratio of the peak ^{13}NN activity in the ROI during apnea, divided by the infused ^{13}NN dose (11). This was multiplied by cardiac output to derive absolute regional perfusion, which was normalized by tissue fraction ($F_{TIS} = 1 – F_{GAS}$) to obtain absolute perfusion per unit tissue ($\dot{Q}_{TIS}$).

3. *Regional Average Lung Inflation (F_{GAS})* – regional fractional gas content at baseline ($F_{GAS,\,BL}$) was computed from baseline transmission scans using a previously described two-point calibration procedure (12).

4. *Fraction of Hyper-Inflated Lung Volume (F_{HI})* – estimated from the respiratory-gated images at end-inspiration. The fraction of hyper-inflated volume (F_{HI}) was defined as the fraction of voxels within a region having $F_{EI}>0.85$.

5. *Fraction of Non-Aerated Lung Volume (F_{NA})* – derived as the fraction of voxels non-aerated at end-inspiration ($F_{EI}<0.1$), indicating tissue continuously collapsed

throughout the respiratory cycle (i.e., stable atelectasis). The use of end-inspiratory images excluded non-aerated lung tissue undergoing tidal recruitment.

6. *Intra-Regional $sV\dot{}$ Heterogeneity ($\sigma_{sV\dot{}}$)* – because our local measurements of sVol obtained with respiratory-gated imaging represent the average tidal strain of lung regions, they provide no information on the distribution of intra-regional strain. However, specific ventilation ($sV\dot{}$) is highly correlated with tidal strain at the regional level and can be measured at the sub-voxel level with ^{13}NN-PET (13-15). Thus, we used the heterogeneity of intra-voxel $sV\dot{}$ as a surrogate measure for the heterogeneity of local tidal strain within each ROI. For this, we analyzed the washout phase of the ^{13}NN infusion scan as previously described (16). Briefly, voxel-level tracer kinetics were fit to four possible models consisting of either one or two compartments, including single-exponential, double-exponential, partial gas trapping, and complete gas trapping models (16). The model with the lowest Akaike Information Criterion (AIC) was chosen for each voxel (17). For each ROI, $sV\dot{}$ heterogeneity ($\sigma_{sV\dot{}}$) was quantified as the standard deviation of the distribution of $\log_{10}(sV\dot{})$ for all voxels within the ROI:

$$\sigma_{sV\dot{}} = SD[\log_{10} sV\dot{}]$$

Values of $sV\dot{} < 10^{-3}$ were set to 10^{-3} to avoid extreme negative numbers resulting from log transformation of small values. For voxels described by two compartments, the fractional contribution of each compartment was computed from its relative perfusion (16).

The effects of these several predictor variables (fractional tidal recruitment, tissue-normalized perfusion, average lung inflation, hyper-inflated tissue, non-aerated tissue, and $s\dot{V}$ heterogeneity) on metabolic activation were assessed by separately modeling k_3 as a function of each predictor variable. Each model allowed for distinct fixed effects of the predictor variable in each group (i.e., interaction of predictor and group) and included random intercepts and predictor effects for each animal, to account for repeated measurements in each animal.

Estimates of Tidal Recruitment and Comparison with ^{18}F-FDG Uptake

Distributions of F_{GAS} at end-expiration and end-inspiration showed only a small amount of atelectasis at baseline in the High-Strain groups ventilated with zero PEEP (Figure S1), as demonstrated by small fractions of voxels in the non-aerated compartment. The Low-Strain group showed close to zero atelectasis, as expected with higher PEEP levels (Figure S1). The amount of atelectasis increased by the end of 3h of mechanical ventilation, particularly in the High-Strain LPS group (Figure S1).

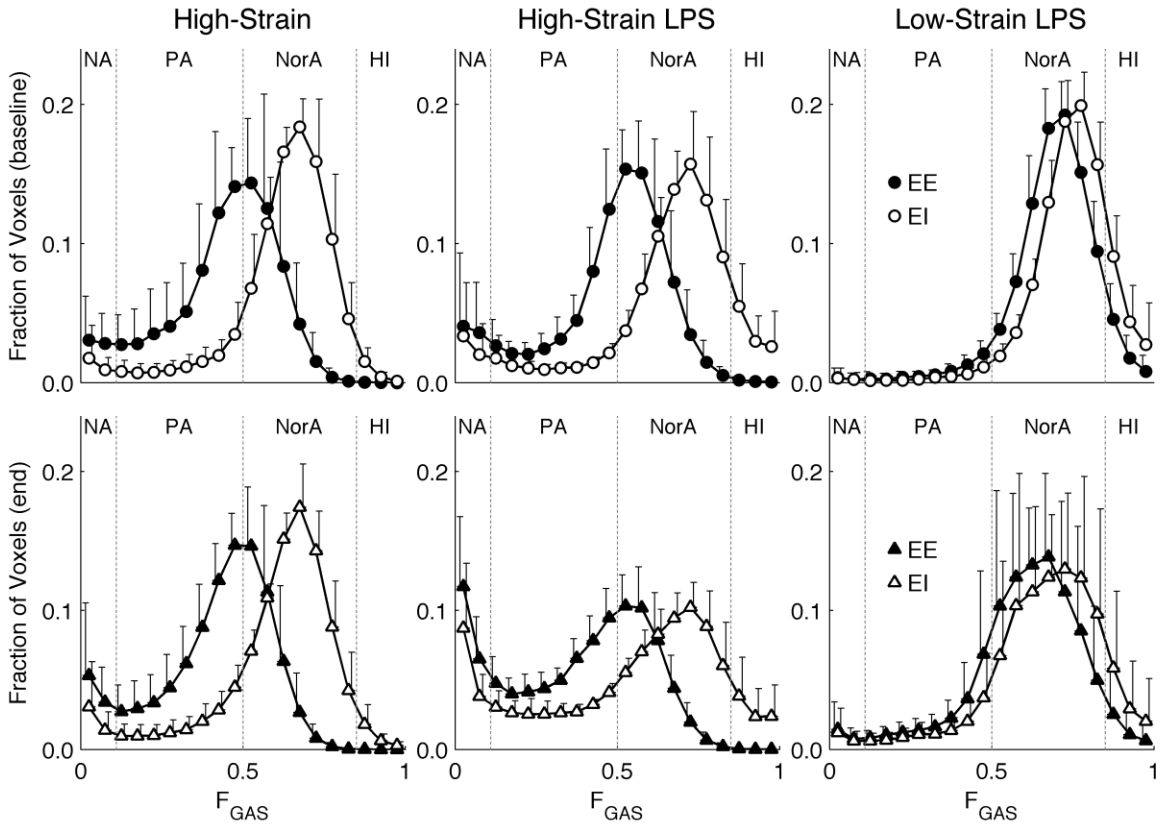

Figure S1. Average (mean±SD) distributions among all animals in each group of voxel F_{GAS} values at end-expiration (EE) and end-inspiration (EI) within the whole imaged lung field. Distributions at baseline (top row) and after 3 hours mechanical ventilation (bottom row) are depicted. Standard CT aeration compartments, including non-aerated (NA), poorly-aerated (PA), normally-aerated (NorA), and hyper-inflated (HI) lung, are separated by dotted lines.

Regional fractions of voxels in the studied aeration compartments showed that atelectasis was confined to dependent lung regions in the High-Strain and High-Strain LPS groups (Figure S2). The decrease in the fraction of lung in the $F_{GAS}<0.1$ and $0.1<F_{GAS}<0.3$ compartments during inspiration (i.e., the tidal recruitment of tissue in these compartments) was small both at baseline and after 3h mechanical ventilation, while the decrease in the $0.1<F_{GAS}<0.3$ compartment was more substantial at both time points (Figure S2).

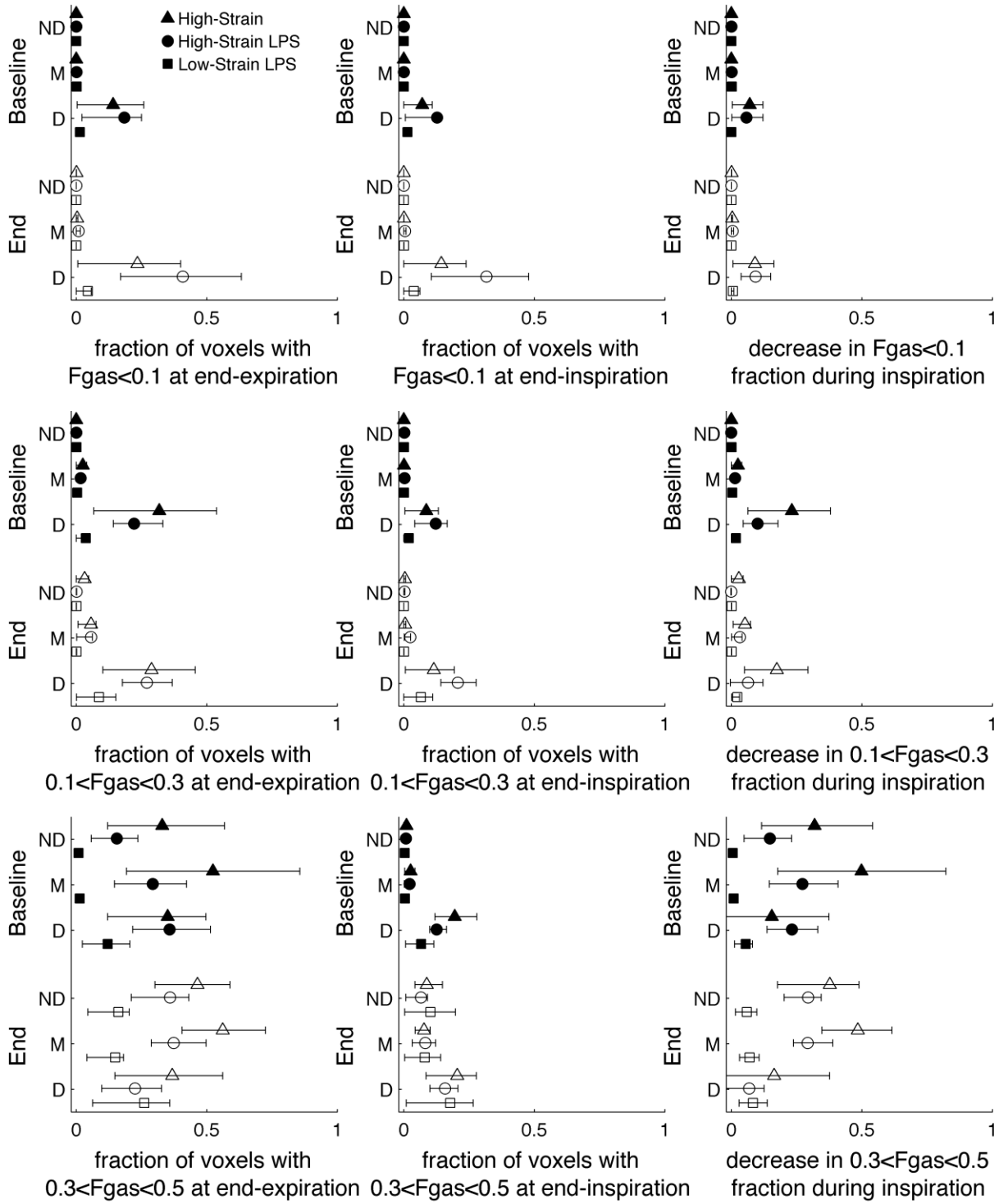

Figure S2. Average regional values (median, 25th and 75th percentiles) of the fractions of lung in F_{GAS}<0.1, 0.1<F_{GAS}<0.3, and 0.3<F_{GAS}<0.5 aeration compartments, as well as the decrease in these fractions during inspiration. All non-dependent (ND), middle (M), and dependent (D) ROIs from each animal and group are shown together at baseline and after 3 hours of mechanical ventilation (end).

Associations between these regional estimates of recruitment and ^{18}F-FDG phosphorylation rate k_3 are shown in Figure 5 of the main text. While no associations between tidal recruitment and k_3 were found in the High-Strain or Low-Strain LPS groups, k_3 was significantly associated with tidal recruitment of the $F_{GAS}<0.1$ compartment ($p=0.019$) and the $0.1<F_{GAS}<0.3$ compartment ($p<0.001$) in the High-Strain LPS group (Figure 5, main text). Thus, tidal recruitment appeared to have no effect on metabolic activation in the High-Strain or Low-Strain LPS groups. In the High-Strain LPS group, recruitment may have been partly responsible for metabolic activation. However, in Table S1, we show that the magnitude of the effect of tidal recruitment was much smaller than the effect of sVol as determined from the mixed-effects model coefficients in each group.

Limitations of Measuring Tidal Recruitment with PET

It should be noted that the respiratory-gated ^{13}NN-PET technique used herein to estimate regional tidal recruitment is not the same as that commonly used to assess recruitment from CT images (18). In fact, there are several key differences between our measurements and those obtained with CT. Firstly, we did not measure changes in the absolute volumes of non-aerated and poorly-aerated tissue, as is usually done with CT (18). Such measurement of absolute volumes is not possible with PET, since (a) the field of view does not include the entire lung, and (b) precise delineation of the same anatomic regions at two distinct lung volumes requires higher resolution. Instead, we examined how the fraction of voxels in each aeration compartment changed with inspiration. The recruitment of collapsed tissue would be expected to reduce the fraction of a given region that is made up of low-aeration voxels. However, changes in these

fractions could also be produced by expansion of normally-aerated tissue or movement of tissue into and out of the defined lung region during inspiration. Whereas we showed that the main component of heterogeneity in aeration in these supine sheep is along the vertical axis, whole-lung quantification would likely increase the accuracy of the results.

Another limitation is that PET has a lower resolution (13 mm after filtering in our respiratory-gated images) than CT (on the order of 1mm (19)), precluding detection of regions of atelectasis underlying that spatial resolution. As a consequence, estimates of lung recruitment would be affected if regions of poorly-aerated tissue detected in our images were composed of juxtaposed normally and non-aerated tissue.

Thus, our estimates of recruitment based on respiratory-gated ^{13}NN-PET imaging need to be interpreted with these limitations in perspective. Given that the resolution limitation is expected to have a limited effect in the current cases since the process of atelectasis in normal lungs has been shown to be distributed approximately homogeneously at that length scale, our estimates suggest that tidal recruitment of non-aerated and poorly-aerated tissue could not have explained our results of a regional dependence of local inflammation on regional strain. It is possible that tidal recruitment contributed to inflammation in the High-Strain LPS group. In this group, surfactant dysfunction associated with endotoxemia may have predisposed the lungs to injury due to recruitment by increasing interfacial stresses experienced by resident cells of the airspaces (20).

Comparison of Functional Variables with ^{18}F-FDG Phosphorylation Rate

No significant associations with k_3 were found for perfusion per unit tissue ($\dot{Q}_{TIS}$) or fraction of hyper-inflated voxels (F_{HI}). Baseline F_{GAS} (average over respiratory cycle) was inversely associated with k_3 in both LPS groups (Figure S3).

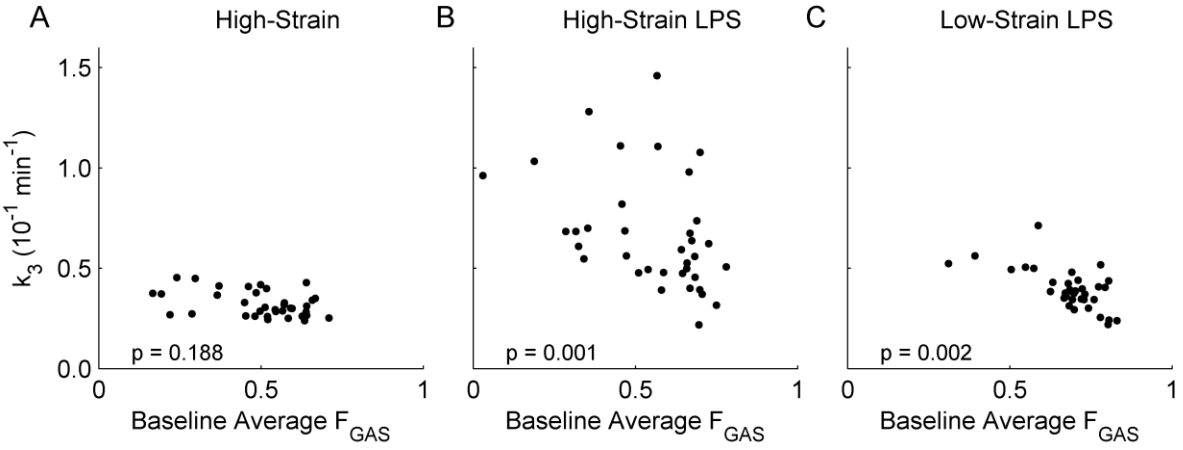

Figure S3. Regional ^{18}F-FDG phosphorylation rate k_3 plotted against average F_{GAS}. Significance of the F_{GAS} effect in the mixed-effects model is shown for each group.

Significant associations were found between k_3 and intra-regional $s\dot{V}$ heterogeneity in the High-Strain LPS and Low-Strain LPS groups (Figure 4B,C), but not in the High-Strain group (Figure S4 A).

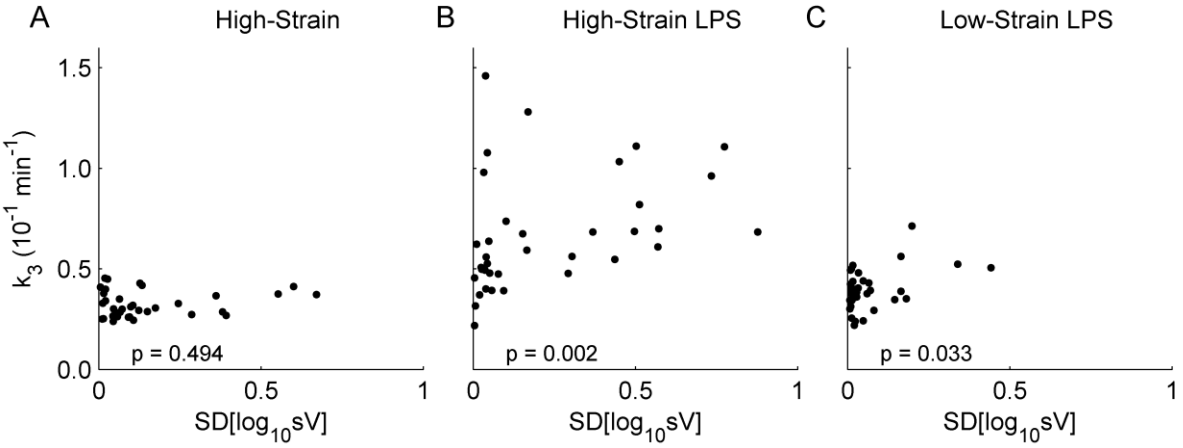

Figure S4. Regional ^{18}F-FDG phosphorylation rate k_3 plotted against the intra-regional heterogeneity of $s\dot{V}$ for each group. Significance of the effect of SD[$\log_{10} s\dot{V}$] in the mixed-effects model is shown for each group.

No associations with k_3 were found for the fraction of non-aerated volume at end-inspiration, $F_{NA,EI}$ (i.e., fraction of region continuously collapsed throughout the respiratory cycle), with most regions showing zero continuous collapse (Figure S5).

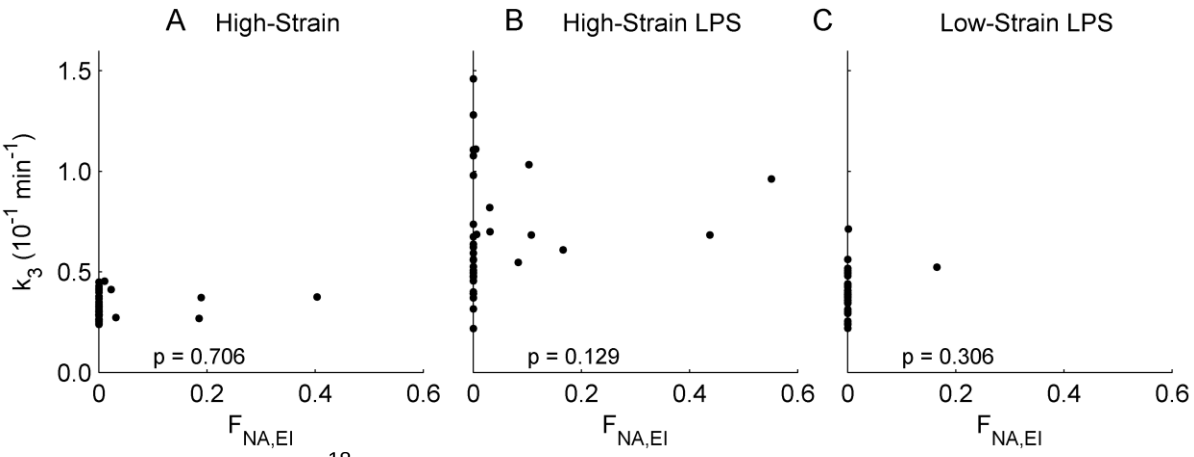

Figure S5. Regional ^{18}F-FDG phosphorylation rate k_3 plotted against the fraction of non-aerated voxels at end-inspiration ($F_{NA,EI}$) for each group. No significant associations were found in any groups with the mixed-effects model.

Comparison of Predictor Variable Effect Magnitudes

In order to compare the relative importance of each of the studied predictor variables for determining regional ^{18}F-FDG phosphorylation rate k_3, we compared the coefficients of each of the predictor variables derived with the mixed-effects models of k_3 after mean-normalizing all predictor variables as well as independent variable k_3 (Table S1). Variables without any significant associations (i.e., tissue-normalized perfusion and fractional hyperinflation) or with negative coefficients (i.e., average F_{GAS}) are excluded from this comparison. Additionally, coefficients of the Low-Strain LPS group are excluded, given the lack of associations of predictors with k_3 in this group.

Table S1. Magnitudes of predictor variable effects in mixed-effects models of k_3.

	High-Strain	High-Strain LPS	Combined LPS
sVol	0.131	0.431	0.395
F_{TR} (F_{GAS}<0.1)	0.009	0.049	0.071
F_{TR} (0.1<F_{GAS}<0.3)	0.019	0.185	0.151
F_{TR} (0.3<F_{GAS}<0.5)	-0.011	-0.046	0.139
SD[$\log_{10}\ s\dot{V}$]	0.024	0.118	0.147

sVol, specific lung volume change (i.e., tidal strain); F_{TR}, fractional tidal recruitment of aeration compartment; F_{GAS}, fractional gas content; SD[$\log_{10}\ s\dot{V}$], heterogeneity of specific ventilation.

For the High-Strain, High-Strain LPS, and combined LPS groups, sVol demonstrated the strongest association with k_3, as indicated by higher predictor coefficients. The coefficient of sVol was more than 5 times larger than the next highest coefficient in the High-Strain group, and more than twice as large as the next highest coefficient in the High-Strain LPS and combined LPS groups. Other predictors with notable coefficient magnitudes were fractional tidal recruitment of the 0.1<F_{GAS}<0.3 compartment and intra-regional $s\dot{V}$ heterogeneity.

References

1. Chu EK, Whitehead T, Slutsky AS: Effects of cyclic opening and closing at low- and high-volume ventilation on bronchoalveolar lavage cytokines. *Crit Care Med* 2004;32:168-174

2. Terragni PP, Rosboch G, Tealdi A, et al: Tidal hyperinflation during low tidal volume ventilation in acute respiratory distress syndrome. *Am J Respir Crit Care Med* 2007;175:160-166

3. Kuebler WM, Kuhnle GE, Goetz AE: Leukocyte margination in alveolar capillaries: Interrelationship with functional capillary geometry and microhemodynamics. *J Vasc Res* 1999;36:282-288

4. Costa EL, Musch G, Winkler T, et al: Mild endotoxemia during mechanical ventilation produces spatially heterogeneous pulmonary neutrophilic inflammation in sheep. *Anesthesiology* 2010;112:658-669

5. Mead J, Takishima T, Leith D: Stress distribution in lungs: A model of pulmonary elasticity. *J Appl Physiol* 1970;28:596-608

6. de Prost N, Costa EL, Wellman T, et al: Effects of surfactant depletion on regional pulmonary metabolic activity during mechanical ventilation. *J Appl Physiol* 2011;111:1249-1258

7. Fernandez-Bustamante A, Easley RB, Fuld M, et al: Regional pulmonary inflammation in an endotoxemic ovine acute lung injury model. *Respir Physiol Neurobiol* 2012;183:149-158

8. Plataki M, Hubmayr RD: The physical basis of ventilator-induced lung injury. *Expert Rev Respir Med* 2010;4:373-385

9. Gattinoni L, Carlesso E, Caironi P: Stress and strain within the lung. *Curr Opin Crit Care* 2012;18:42-47

10. Gattinoni L, Pelosi P, Crotti S, et al: Effects of positive end-expiratory pressure on regional distribution of tidal volume and recruitment in adult respiratory distress syndrome. *Am J Respir Crit Care Med* 1995;151:1807-1814

11. Schroeder T, Vidal Melo MF, Musch G, et al: PET imaging of regional 18F-FDG uptake and lung function after cigarette smoke inhalation. *J Nucl Med* 2007;48:413-419

12. Harris RS, Willey-Courand DB, Head CA, et al: Regional VA, Q, and VA/Q during PLV: Effects of nitroprusside and inhaled nitric oxide. *J Appl Physiol* 2002;92:297-312

13. Reinhardt JM, Ding K, Cao K, et al: Registration-based estimates of local lung tissue expansion compared to xenon CT measures of specific ventilation. *Med Image Anal* 2008;12:752-763

14. Fuld MK, Easley RB, Saba OI, et al: CT-measured regional specific volume change reflects regional ventilation in supine sheep. *J Appl Physiol* 2008;104:1177-1184

15. Wellman TJ, Winkler T, Costa EL, et al: Measurement of regional specific lung volume change using respiratory-gated PET of inhaled 13N-nitrogen. *J Nucl Med* 2010;51:646-653

16. Wellman TJ, Winkler T, Costa EL, et al: Effect of regional lung inflation on ventilation heterogeneity at different length scales during mechanical ventilation of normal sheep lungs. *J Appl Physiol* 2012;113:947-957

17. Landaw EM, DiStefano JJ,3rd: Multiexponential, multicompartmental, and noncompartmental modeling. II. data analysis and statistical considerations. *Am J Physiol* 1984;246:R665-77

18. Caironi P, Cressoni M, Chiumello D, et al: Lung opening and closing during ventilation of acute respiratory distress syndrome. *Am J Respir Crit Care Med* 2010;181:578-586

19. Kaczka DW, Cao K, Christensen GE, et al: Analysis of regional mechanics in canine lung injury using forced oscillations and 3D image registration. *Annals of Biomedical Engineering* 2011;39:1112-1124

20. Hussein O, Walters B, Stroetz R, et al: Biophysical determinants of alveolar epithelial plasma membrane wounding associated with mechanical ventilation. *Am J Physiol Lung Cell Mol Physiol* 2013;305:L478-84